Revised Manuscript

Ferroelectric Behavior in Exfoliated 2D Aurivillius Oxide Flakes of Sub-Unit Cell Thickness

***Lynette Keeney*[1]*, *Ronan J. Smith*[2], *Meghdad Palizdar*[3], *Michael Schmidt*[1], *Andrew J. Bell*[3], *Jonathan N. Coleman*[2] and *Roger W. Whatmore*[4, 5].

1. Tyndall National Institute, University College Cork, 'Lee Maltings', Dyke Parade, Cork, Ireland.
2. School of Physics and Centre for Research on Adaptive Nanostructures and Nanodevices, Trinity College, Dublin, D2 Dublin, Ireland.
3. Institute for Materials Research, University of Leeds, Leeds LS2 9JT, United Kingdom.
4. Department of Chemistry, University College Cork, Cork, Ireland.
5. Department of Materials, Faculty of Engineering, Imperial College London, London, SW7 2AZ, United Kingdom.

Abstract

2D materials, which are self-supporting in large areas but are only a few atoms thick, are exciting considerable interest for potential applications as diverse as electronics, molecular filtration and structural materials. Ferroelectrics have many useful applications stemming from their electrically-switchable dielectric spontaneous polarizations, including in piezoelectric devices, non-volatile memories and pyroelectric IR sensors. While 2D oxide materials are known, they have not yet received the same attention as materials such as graphene. Here we study the ferroelectricity in ultrasonically-exfoliated flakes of the layered Aurivillius oxide $Bi_5Ti_3Fe_{0.5}Co_{0.5}O_{15}$ with a range of thicknesses. We show, for the first time, that ferroelectricity can exist in flakes with thicknesses of only 2.4nm, which is about one-half of the normal crystal unit cell. These flakes have relatively large areas (linear dimensions many times the film thickness), thus classifying them as 2D materials. Piezoresponse force microscopy (PFM) has been used to show that these very thin flakes both

exhibit piezoelectric effects and that the ferroelectric polarization can be reversibly switched. A new model is presented that permits the accurate modelling of the field-on and field-off PFM time-domain and hysteresis loop responses from a ferroelectric during switching in the presence of charge injection, storage and decay through a Schottky barrier at the electrode-oxide interface. This allows the extraction of parameters such as the coercive fields (E_C), electrostrictive coefficients (Q_{11}) and spontaneous polarizations (P_S) for the flakes. It is found that the values of P_S are around 0.04(±0.02)Cm^{-2}, and Q_{11}=2(±0.1)x$10^{-2}m^4C^{-2}$. These are in good agreement with other ferroelectric Aurivillius oxides. E_c scales with thickness (t), closely following the semi-empirical scaling law expected for ferroelectric materials, vis: $E_C \propto t^{-\frac{2}{3}}$. We believe this constitutes the first evidence for ferroelectricity in a 2D oxide material, and it offers the prospect of new devices that might use the useful properties associated with the switchable ferroelectric spontaneous polarization in a 2D materials format.

Introduction

2D materials, such as graphene, have received enormous attention over the last 10 years for their huge potential range of applications, ranging from electronics and photonics to structural materials, as has been comprehensively described elsewhere.[1] The definition of a 2D material as being one of large area but only one atom thick (e.g. graphene) has been relaxed to include materials which can exist in large area, but a few atoms and typically ca 1 unit cell or less in thickness[1a] and being self-supporting (without the necessity for a substrate). As a consequence, many 2D materials apart from graphene are being studied, such as the MoS_2 family. Many of these materials are semiconductors. A variety of manufacturing techniques exist[1b], including mechanical exfoliation and direct growth. Liquid exfoliation (high shear & ultrasonic) methods offer the prospect for the low-cost production of large volumes of flakes in suspension that can subsequently be used in a variety of ways.[2] 2D functional oxides also exist and examples include simple transition metal oxides such as titania[3] and perovskite[4] $La_{0.95}Nb_2O_7$ nanosheets made by exfoliation, which have been studied for their potentially-high relative permittivities (45 to 100),[5] MnO_2 flakes which have received attention for battery[6] and supercapacitor applications[7] and layered tantalates such as $H_{1.81}Sr_{0.81}Bi_{0.19}Ta_2O_7$ being investigated for photocatalytic water splitting.[8] Recently, it has been shown that mechanically-exfoliated 2D flakes of the oxide superconductor $Bi_2Sr_2CaCu_2O_{8+\delta}$ exhibit superconducting transition temperatures similar to the bulk when only one-half a unit cell in thickness.[9]

Ferroelectrics (FEs) offer a range of functional properties[10] and are widely used in e.g. non-volatile memories,[11] piezoelectric RF Filters[12] and pyroelectric infra-red detectors.[13] FE switching has previously been reported in very thin films e.g. 7.5nm PVDF-TrFE copolymer films[14] and films of $BaTiO_3$ as thin as 3nm (ca 8 perovskite unit cells or "blocks").[15] Recently, FE behavior has been reported in free-standing monolayer flakes of In_2Se_3[16] and $MoTe_2$[17] although their spontaneous polarizations (P_S) have not been quantified and the difficulties of measuring P_S in such narrow band-

gap materials are widely acknowledged.[18] The Aurivillius oxide layer-structure materials (APMs)[19] - general formula $Bi_2O_2(A_{m-1}B_mO_{3m+1})$ - consist of *m* perovskite ABO_3 blocks interspersed with fluorite Bi_2O_2 layers. Many APMs are FE, e.g. $Bi_4Ti_3O_{12}$.[20] Characteristically, they have high Curie temperatures (>600°C), large in-plane P_S (ca $0.4Cm^{-2}$) and in some cases small out-of-plane P_S. $SrBi_2Ta_2O_9$ (m = 2) and $Bi_{3.25}La_{0.75}Ti_3O_{12}$ (m = 3) APMs have been developed for commercial use in Fe-RAM (FE random access memory) devices.[21] APMs are structurally-flexible, as many different cations can be included in the perovskite layers, and *m* can be varied from two up to nine.[22] [23]

APMs are amenable starting materials for exfoliation into 2D nano-sheets.[24] However, to date there have been no studies reported of the FE properties of exfoliated APM nanoflakes. Here we report, for the first time, the study of ferroelectricity in thin exfoliated nanoflakes of the APM $Bi_5Ti_3Fe_{0.5}Co_{0.5}O_{15}$ (B5TFCO) (m = 4) using piezoresponse force microscopy (PFM), with flake thicknesses ranging from ca 100nm down to 2.4nm. We present a model which allows extraction of the important FE parameters such as the coercive fields (E_C), electrostrictive coefficients (Q_{11}) and spontaneous polarizations (P_S) in the presence of charge injection, storage and leakage with Schottky barriers at the FE oxide-electrode interfaces. We demonstrate FE switching in all the exfoliated B5TFCO nanoflakes. The switching shows very similar characteristics right across the thickness range, and persists in flakes with thicknesses of 2.4 nm and high aspect ratios (diameter 80 nm). This thickness corresponds to just over one-half unit cell or four perovskite oxide blocks plus the associated Bi_2O_2 layers. We believe this demonstrates for the first time that the class of self-supporting 2D oxide materials can include FEs, with all their useful functional properties, greatly increasing the potential range of their applications.

Characterization of Dispersed $Bi_5Ti_3Fe_{0.5}Co_{0.5}O_{15}$ (B5TFCO) Nanoflakes

B5TFCO has orthorhombic symmetry with lattice parameters a=0.5373nm, b=0.5430nm and c=4.1268nm, as illustrated in Figure 1.[25] Exfoliated nanoflakes were made by ultrasonic exfoliation in a liquid[26] (see Methods) from highly-oriented molten-salt synthesized ceramics.[27] These were dispersed onto Ti-coated Si substrates (see Methods) and characterized using SEM, TEM, AFM and

PFM. SEM analysis reveals that the dispersed nano-structured flakes have plate-like morphologies, which is characteristic of the layered Aurivillius-type structures. A range of flake sizes (lateral diameters of 80 nm to 700 nm) can be observed in the SEM images (see Figure S1 for an example) as individual flakes, or stacked on top of each other or overlapped together in clusters. The two larger particles shown in Figure S1 were chosen for FIB cross-sectioning. Cross-sectional HR-TEM images of these (**Figure S2**) shows that these particles are clusters of flakes. Figure S2 shows the lattice images taken from these. It shows clear evidence for the expected 4-perovskite-block APM structure possessing a unit cell 4.1 nm long (*c*-axis), consistent with Figure 1. The TEM data **Figure S2** shows that the larger clusters of flakes can be clustered in multi-flake aggregates.. van der Waals forces position the majority of the flakes closely parallel to the substrate surface although not all crystals are aligned perfectly flat. STEM-EDX analysis confirmed the presence of Bi and Ti in approximately the correct proportions, with the presence of low levels of Fe and Co as expected from the B5TFCO composition. This, in association with the TEM lattice images, confirms that the larger flakes maintain the APM structure. We will show that the electrical properties of the thicker flakes scale well with thickness, right down to the thinnest flakes. We believe that this is good evidence that the APM structure is maintained down to the thinnest flakes. **Figure 2** presents evidence that thinner flakes can be found which are not clusters. Here we present (**Figure 2a**) an AFM topographic image of a single 15nm flake of B5TFCO which is lying flat in the substrate. This is nearly circular and approximately 250nm in diameter, giving it a diameter-to-thickness aspect ratio of ca17:1.

Electromechanical responses of the exfoliated B5TFCO flakes were assessed by simultaneous lateral and vertical PFM measurements, respectively, at a single drive frequency of 20kHz. **Figure S3** shows the topography (**Figure S3a**) of a flake ~300nm in diameter and ~33nm in height, together with the in-plane (**Figure S3b** – amplitude, **e** - phase) and out-of-plane (**Figure S3c** - amplitude, **f** - phase). It is clear from the single frequency PFM images that higher piezoresponses are obtained in the lateral direction (11 pmV^{-1}) compared with those measured in the vertical direction (3 pmV^{-1}). This is expected, given that the major polarization vector for APMs is along the *a*-axis.[28] The

enhanced lateral PFM response confirms that the majority of the flakes are preferentially *c*-axis oriented, with their crystallographic *a*-axes lying in the lateral plane of the film. . Given the relatively low piezoresponses, topography cross-talk is likely also to have some contribution to the single frequency vertical PFM images obtained. In order to amplify the weaker vertical piezoresponse and reduce effects of topography cross-talk, the DART-PFM mode was used (see Methods). [29]The intensified amplitude and phase responses are displayed in **Figure S3d** – amplitude **& g** – phase, respectively. The magnitude of the out-of-plane response is discussed further below.

In order to investigate size effects on the electromechanical properties of the exfoliated B5TFCO nanoflakes, vertical DART-PFM imaging was performed on flakes with a range of lateral dimensions (230nm to 2μm) and thicknesses (14nm to 120nm). **Figures 2b & c** show the vertical amplitude and phase responses from the same flake for which the topography image is shown in **Figure 2a**. The response appears to be remarkably uniform in both amplitude and phase, and indicative that this flakes is single domain, although evidence for multi-domain structures was observed in other flakes.

[30]Investigation of local room temperature FE switching in the nano-sized flakes was performed by vertical DART-PFM switching spectroscopy measurements at a distinct tip position after the removal of an applied pulsed DC bias (“field off state”) (**Figure 2**). Note that the “field on” loops are not presented here, since electrostrictive effects and electrostatic interactions between the cantilever and the back electrode can complicate the interpretation of the hysteresis loops obtained. However, they are presented and discussed further below. Evidence is presented here for FE hysteresis (**Figure 2d**) and 180° FE switching between two antiparallel polarization states (**Figure 2e**) is indicated for flakes from 100nm thick down to thicknesses of 14nm. Vertical DART-PFM switching spectroscopy was also conducted on much-thinner individual flakes, as shown in **Figures 3a, b, c**. These vertical DART-PFM measurements demonstrate piezoelectricity in nano-structured B5TFCO flakes with thickness of 8nm (which corresponds to 2 unit cells of B5TFCO) and diameter of 160nm. Note that this flake appears to have two domains (indicated by areas with a 180° phase shift

between them) and with a domain wall running approximately vertically down the center of the flake. The presence of different domain structures has previously been demonstrated[30] for nanodots of similar geometry but with irregularities in shape and strain. The multi-domain character may be helping to stabilize the piezoresponse at these smaller dimensions.

Ferroelectricity was investigated for this and other individual flakes: 4.2nm thick / 100 nm diameter (aspect ratio 24:1) and 2.4nm thick / 80nm diameter (aspect ratio 33:1), as demonstrated by the piezoresponse and phase vertical DART-PFM switching spectroscopy hysteresis loops (**Figure 3d**,**e** respectively). 180° FE switching is observed in all cases. The smaller flake thicknesses correspond to one unit-cell and to just over half a unit cell of B5TFCO, respectively. Note that one edge of the 4.2 nm thick flake has overlapped on top of the 2.4 nm flake and is therefore somewhat tilted. These flakes were initially imaged in contact mode AFM (no AC bias) to obtain the topography images inset in **Figure 3d,e**. Following this, DART-PFM switching spectroscopy hysteresis loops were obtained. PFM imaging (i.e. scanning the PFM tip while applying an AC drive voltage) of the smaller flakes (4.2 nm and 2.4 nm in height) could not be obtained because the process caused physical damage. Large-scale surface damage at increased bias has previously been reported for PZT ($PbZr_{0.52}Ti_{0.48}O_3$) nanodots.[31]

APMs are well-known FEs and ferroelectricity has been established for Co-substituted $Bi_5Ti_3FeO_{15}$ ceramics and thin film samples.[27, 32] However, the fact that ferroelectricity has been established for larger structures is not proof that ferroelectricity will exist at smaller dimensions. We now consider the results of the PFM experiments to ascertain if they support FE behavior, considering that other contributions (e.g. electrostatic effects, electrostrictive effects, surface electrochemical reactions, charge migration effects)[33] can affect the PFM signals. We note that the loops follow the typical counterclockwise behavior expected for standard FEs.[33] The piezoresponse versus applied voltage PFM loops for the B5TFCO flakes were performed in a pulsed DC mode which minimizes electrostatic and electrostrictive contributions to the signal[34]. However, measurement of loop evolution with V_{ac} (drive amplitude) is a necessary step to establish the validity of PFM

hysteresis measurements.[35] For most electromechanically active materials with dominant piezoelectric coupling and weak electrostrictive contributions, when below the coercive voltage of the material, the piezoresponse amplitude is directly proportional to V_{ac} while the piezoresponse phase is V_{ac} independent.[36], [33] Linearity of piezoresponse (pm) with drive amplitude (V_{ac}) was verified for a flake of 76nm height and 579nm diameter at a constant DC bias of 15 V (**Figure S4**).

PFM Response Modelling

An interesting aspect to the hysteresis loops observed from the exfoliated flakes and shown in **Figures 2** and **3** is their shape at high voltages. The piezoresponse is observed to increase at high voltage, rather than to saturate, as would be expected for a perfect switched FE. The shape is reproducible across the series of flake thicknesses and applies to both flake aggregates and single crystals. This type of loop shape has been reported before from a range of materials, including PFM data from thin films of e.g. $BiFeO_3$,[37] strain-free $SrTiO_3$[38] and P/E loops from PVDF-TrFE films and composites with 5%$BiFeO_3$-$NaNbO_3$ powders,[39] although hitherto it has not been explained. It is likely that the effect observed is due to the injection of charge from the electrodes into the FE after the switching of polarization in both positive and negative senses, creating a layer of trapped, but mobile, charge (electrons or holes) that increases the local polarization and thus the piezoresponse. However, when the field is removed the charge might be expected to leak away, and this is what we observe.

To understand the detailed shape of the PFM loops (and, indeed the whole of the field-on, field-off response), we need to consider in detail how the PFM experiment is performed. Starting from zero applied field, a small AC voltage is applied to the PFM tip, and the piezoresponse is measured in individual time slots ⍰t (e.g. ⍰t=0.5ms). N (say N=50) readings are taken at zero applied bias, giving a total field-off measurement time of ⍰t=N.⍰t (25ms in this example). This is the first “field-off” response measurement. A DC bias (V_1) is applied for a time ⍰t (in this example for 25ms) and a further N (50) “field-on” response measurements are taken. The DC bias is removed and a further N (50) “field-off” response measurements taken. These are the “field-off” piezoresponse

readings corresponding to V_1, with the readings being averaged over a pre-set number of the 50 readings taken. This process is repeated with V_1 increased (or decreased) by an amount ⍰V, to give the full hysteresis loop. The parameters ⍰t, N and ⍰V can all be varied within the PFM instrument parameters. To model the piezoresponse behavior in the presence of mobile charge injection and leakage, consider how the charge will move into and out of the FE during the field-on and field-off periods, taking account of the switching of the FE polarization through the loop cycle. To do this, we use the approach of Pintilie and Alexe[40], later modified by Fan et al.[41], who considered the thermionic emission of current into an insulator across a metal-insulator junction, including the effects of FE polarization and charge trapping. The descriptions are based on a modified version of the Schottky barrier model.

The energy bands at a Schottky contact between a metal and an insulator (or semiconductor) are illustrated as in **Figure 4a**[41]. ϕ_B^0 is Schottky barrier height set by the Fermi level in the metal, V_{bi} is the height of the built-in potential barrier and w is the width of the Schottky depletion region. In **Figure 4b** we see the description of the barrier in the presence of the FE polarization *P*. The FE is assumed to have been poled by the application of a negative voltage to the metal, so the FE polarization can be treated as a sheet of positive charge situated at a depth δ below the metal-FE interface. This is called "negatively poled" and denoted $P\uparrow$ and changes (in this case increases) V_{bi} to some value V_{bi}' and the ϕ_B^0 is increased to ϕ_{App}. The converse poled case is shown in **Figure 4c**. The layer defined by δ is sometimes referred to as the "dead layer". Fan et al.[41] assume that charges injected into the FE become trapped and reside in the dead layer with a volumetric density $N_{Trapped}$ to give a total charge $Q_{Trapped}$, (in Cm^{-2}) given by:

$$Q_{Trapped} = qN_{Trapped}\delta \qquad (1)$$

Where q is the electron charge.

The following equations are derived by Fan et al.[41] They are very similar to the equations derived by Pintilie and Alexe[40] but include the effects of the charge trapped in the dead layer.

$$V'_{bi} = V_{bi} \mp \frac{P}{\varepsilon_0 \varepsilon_{st}} \delta \pm \frac{qN_{Trapped}}{2\varepsilon_0 \varepsilon_{st}} \delta^2 \qquad (2)$$

$$V_{bi} = \phi_b^0 - \frac{k_B T}{q} ln\left[\frac{N_V}{p(T)}\right] \qquad (3)$$

In the above, ε_0= permittivity of free space; ε_{st}=low frequency permittivity of FE, k_B=Boltzmann's Constant; N_V=Density of states for holes in the valence band; $p(T)$= Hole concentration at temperature *T*.

The depletion width is given by:

$$w = \left(\frac{2\varepsilon_0 \varepsilon_{st}(V+V'_{bi})}{qN_{eff}}\right)^{\frac{1}{2}} \qquad (4)$$

Here, V=applied voltage and N_{eff}=effective charge density in the films.

The maximum field at the interface is given by:

$$E_m = \frac{qN_{eff}w}{\varepsilon_0 \varepsilon_{st}} \pm \frac{P}{\varepsilon_0 \varepsilon_{st}} \mp \frac{qN_{Trapped}}{2\varepsilon_0 \varepsilon_{st}} \delta \qquad (5)$$

In equations (2) and (5), the lower signs apply to the case of a negatively poled FE where $P \uparrow$ and the upper signs for the reverse case.

This can be put into a form that eliminates w:

$$E_m = \left[\frac{2qN_{eff}(V+V'_{bi})}{\varepsilon_0 \varepsilon_{st}}\right]^{\frac{1}{2}} \pm \frac{P}{\varepsilon_0 \varepsilon_{st}} \mp \frac{qN_{Trapped}}{2\varepsilon_0 \varepsilon_{st}} \delta \qquad (6)$$

The apparent barrier height is given by:

$$\phi_{App} = \phi_B^0 - \sqrt{\frac{qE_m}{4\pi\varepsilon_0 \varepsilon_{opt}}} \qquad (7)$$

Where ε_{opt}=optical frequency permittivity of FE

In the presence of strong carrier recombination, Pintilie[40] quotes:

$$J = qN_V \nu_D \exp\left(\frac{-q\phi_{App}}{k_B T}\right) \quad (8)$$

Where ν_D is the carrier diffusion velocity which is proportional to the carrier drift mobility μ_D. This can be rewritten as:

$$J = qN_C \mu_D E_m \exp\left(\frac{-q\phi_{App}}{k_B T}\right) \quad (9)$$

Where N_C is the density of carriers available for the drift into the charge traps. This is likely to be mediated via a hopping process so that the current density is “bulk limited”, rather than being limited by thermionic emission into the FE from the electrodes.

Based on the previous observation that μ_D is strongly dependent on temperature, we assume that μ_D is determined by some sort of thermal activation process and an equation of the form:

$$\mu_D = \mu_D^o \exp\left(\frac{A}{k_B T}\right) \quad (10)$$

To model the space charge contribution to the PFM response, we assume that during the “field-on” part of the PFM cycle, some space charge is injected into the sample, with a current as determined by the Schottky barrier model described above. This adds to the sheet polarization due to the FE polarization. During the “field-off” part of the cycle, the space charge will tend to leak away with a certain time constant that will depend on the electrical conductivity of the system, permittivity etc. This will give an exponential-decay function. We assume that in each part of the field-on cycle, the charge is injected to give a trapped charge:

$$Q_{Trapped} = J\Delta t \quad (11)$$

Where Δt=”field-on” time as defined above.

This will add to the total polarization P_T in the system, so that:

$$P_T = P + Q_{Trapped} \quad (12)$$

During a field-off cycle, the magnitude of the piezoelectric coefficient d_{eff} is then given in terms of the electrostrictive coefficient Q_{11} by:

$$d_{eff} = 2Q_{11}P_T\varepsilon_0\varepsilon_{st} \quad (13)$$

During a "field-on" cycle, the applied voltage induces a further polarization P_{ind}, which is given by:

$$P_{ind} = V\kappa\varepsilon_{eff}\varepsilon_o/t \quad (14)$$

Where κ is a variable introduced to allow for effects of FE thickness, tip geometry etc. on the induced polarization.

During the field-on cycles, the sign of P_{ind} is observed to be opposite to the sign of P_T.

$$d_{eff} = 2Q_{11}(P_T - P_{ind})\varepsilon_0\varepsilon_{st} \quad (15)$$

In making a calculation for d_{eff}, we also need to take account of the fact that the "dead-layers" at each FE-metal interface are non-FE, low permittivity materials. These place two capacitors in series with the active FE layer, which reduces the AC field across the FE, and hence the measured d_{eff}, by a factor F_{Red}:

$$F_{Red} = \left(\frac{\varepsilon_{st}}{\varepsilon_{opt}}\frac{1}{\left(\frac{t}{2\delta}-1\right)} + 1\right)^{-1} \quad (16)$$

We also need to take account of the way the trapped charge leaks away during both the field-on and field-off cycles. This accomplished by applying an exponential charge leakage term. To model the time structure, we split each field-on and field-off period into a number of N steps (e.g. 50). We assume that the injected current is constant throughout each step period. (This is an approximation as the current is affected to some extent by the number of trapped charges.) The $N_{Trapped}$ (and hence the value of $Q_{Trapped}$) at the end of each period Δt is calculated in the following way:

1. The $N_{Trapped}$ is given a starting value for V=0, say $N^0_{Trapped}$. This is chosen to be equal to the value at the end of a complete cycle when the voltage again returns to zero. It is found that the result is not strongly dependent on the value chosen for $N^0_{Trapped}$.
2. During each section m of a field-on period, the value of $N_{Trapped}$ is calculated as:

$$N_{Trapped}^{m} = \frac{J\Delta t}{q\delta} + N_{Trapped}^{m-1}\exp(-\gamma\Delta t) \quad (17)$$

Where γ is a decay constant and $N_{Trapped}^{m-1}$ is the number of carriers trapped at the end of the previous period. J is calculated using equations (6) and (9) with the value of $N_{Trapped}$ in equation (6) being set as the value of $N_{Trapped}^{m-1}$.

3. During each section m of a field-off period, the value of $N_{Trapped}$ at the end of each section m is calculated as:

$$N_{Trapped}^{m} = N_{Trapped}^{m-1}\exp(-\gamma\Delta t) \quad (16)$$

The value of $N_{Trapped}^{m}$ at the end of each period is used to calculate the trapped charge density from:

$$Q_{Trapped} = N_{Trapped}^{m} q\delta \quad (17)$$

This is then used in equations (12) to (15) to calculate d_{eff} throughout the field-on and field-off cycles.

In their modelling, Fan et al.[41] used a square hysteresis loop. Real FEs are almost-never so well-behaved, and in this model the values of the FE polarization as a function of field used in Equations (5) and (6) are derived using the semi-empirical tanh function described by Miller et al.[42] and Blom et al.[43] Here, the polarization *P(E)* is described as a function of the electric field *E* using:

$$P(E) = \varepsilon_0(\varepsilon_{opt} - 1)E + P_S\tanh[\frac{E \pm E_c}{2\alpha}] \quad (18)$$

Where P_S=Spontaneous Polarization, P_R=Remanent Polarization, E_c=Coercive Field and:

$$\alpha = E_c\left[ln\frac{1+\beta}{1-\beta}\right] \quad \beta = \frac{P_R}{P_S} \quad (19)$$

This produces a loop as illustrated in **Figure S4**. In this graph, the "positive going" arm of the loop takes the minus-sign in the tanh function in Equation (18), while the "negative going" arm of the loop takes the plus-sign. Loop shifts (either in the polarization or voltage axes) caused by in-built biases (charge or voltage asymmetries) are frequently observed in FE thin films (Refs). In this model we have allowed for the possibility of loop displacements in either the voltage or polarization axes by introducing the parameters P_{Shift} and V_{Shift}.

In our model, we use the following parameters for all the examples:

$N_V = N_C$ = 2x10^{28}m^{-3} ; N_{eff}= 4x10^{28}m^{-3} $p(300)$ = 5x10^{24}m^{-3}; Φ_B^0=1.3eV (these are similar to the values used by Fan et al. for PZT films[41]). $N_{trapped}(t = 0)$ = 10^{21}m^{-3}

The low frequency permittivies ε_{st} have been measured for a range of Aurivillius oxides, and the values are quite similar. These include 140 for $CaBi_4Ti_4O_{15}$[44], and 160 for hot-forged $Bi_4Ti_3O_{12}$[45]. A value of ε_{st}=140 has been used here. A refractive index of 2.7 in $Bi_4Ti_3O_{12}$ has been measured by Cummins[46], corresponding to an optical permittivity of 7.3. We have used a value of ε_{opt}=6.5 in this model. The value of δ (dead layer thickness) was fixed at 0.035nm, similar to the value derived by Dawber et al.[47] in their modelling of dead layer thicknesses and polarization field correction in FE switching in PVDF, and the value fits well with our observations.

The parameters V_C (coercive voltage), V_{Shift} , P_S , $\Delta P_R = P_S - P_R$, P_{Shift} , μ_D (carrier drift mobility), γ (charge decay constant), ε_{eff} (effective permittivity) and Q_{11} (electrostrictive coefficient) were fitted parameters. These were fitted by a process of least-squares (minimizing $r^2 = \sum(d_{obs} - d_{calc})^2 / \sum(d_{obs}^2)$) over the full field-on and field-off data for measurements of d_{eff}. Two data points were ignored on each side of the voltage switching transient, so 46 data points were fitted in each field-on or field-off period, and the models were fitted over one-and-one-half full voltage cycles so nearly 10,000 data points were taken for each fitting. Note that the first half-cycle was ignored as this serves to polarize the point on the flake in a particular direction. It was observed that Q_{11} = 2(±0.1)x10^{-2}m^{4}C^{-2}. This is in the middle of the range observed for FE perovskite titanates[48].

FE and butterfly loops were plotted by taking the average of the last 10 d_{eff} values in each field-off period, for both the observed and modelled values and plotting them against the applied voltage value in the immediately-preceding field-on period.

The results of the fitting for a 30nm thick flake are shown in **Figure 6**. It can be seen that the model describes the behaviour of d_{eff} well, in both the time-structure and around the butterfly and

hysteresis loops. The parameters derived from the fitting process, and the r^2 values for each fit, are given in **Table S1**.

Figure 7 shows comparisons between the observed and modelled PFM piezoresponse data for flakes of 2.4, 4.2, 8 and 14nm thickness, together with the time-structure PFM response for the 2.4nm flake, including an example where we have "zoomed-in" on part of the time structure. The agreement between the modelled and observed data is very good for both the PFM loops and the field-on and field-off time structures. If we look in detail at the materials parameters used to model the data, we find that the low frequency (ε_{st}) and optical (ε_{opt}) permittivities used (140 and 6.5) are in excellent agreement with parameters for similar materials in the literature: ε_{st} =140 for $CaBi_4Ti_4O_{15}$[44], and 160 for hot-forged $Bi_4Ti_3O_{12}$[45] and ε_{opt}=7.5 in $Bi_4Ti_3O_{12}$ (Cummins[46]). The value of δ (dead layer thickness) used in our model was fixed at 0.035nm. This is similar to the value derived by Dawber et al.[47] in their modelling of dead layer thicknesses and polarization field correction in FE switching in PVDF. We observed that Q_{11} = 2(±0.1)x10^{-2}m^{4}C^{-2}. This is in the middle of the range observed for FE perovskite titanates[48]. Based on an out-of-plane spontaneous polarization of 0.04Cm^{-2} observed by Takenaka[45] in hot-forged $Bi_4Ti_3O_{12}$, ε_{st} =160 and a Q_{11} = 2x10^{-2}m^{4}C^{-2} we calculate for that material an out-of-plane piezoelectric coefficient *d* of 2.3pmV^{-1}. This is in excellent agreement with the values obtained at zero applied voltage for the 14nm thick flake shown in **Figure 4d**. The thinner flakes show somewhat smaller values of *d*. The parameters extracted from the fitting of the model to the observed data on all the flakes studies are given in **Table S1**. The values of P_S are not strongly dependent on flake thickness, showing a good deal of scatter, which is what would be expected if some of the flakes were slightly canted out of the plane. We observe an average value of 0.04(±0.02)Cm^{-2}. The mean value is in very good agreement with the value observed for $Bi_4Ti_3O_{12}$, as reported above, although this may simply be a coincidence, as discussed below.

1
2
3
4
5
6
7
8
9
10
11
12
13
14
15
16
17
18
19
20
21
22
23
24
25
26
27
28
29
30
31
32
33
34
35
36
37
38
39
40
41
42
43
44
45
46
47
48
49
50
51
52
53
54
55
56
57
58
59
60
61
62
63
64
65

We do not see a strongly systematic variation of either the drift mobility (average μ_D=1.4x10^{-6} m^{2}V^{-1}s^{-1}) or the charge decay constant (average γ = 18s^{-1}) with flake thickness (see **Table S1)**. The dependence of these parameters on temperature, and the comparison of flakes with thin films, will be the subject of a further publication.

Figure 7a shows the variation of the coercive field E_C with thickness. (Here, we have taken the mean values of E_C for all the 33nm thickness measurements conducted at different maximum applied voltages V_{Max}). Empirically, E_C increases with decreasing thickness of the FE material[47]. As explained by Ducharme et al.[49] the extrinsic coercive field observed in FEs is caused by localized nucleations of domains with reversed polarization. Defects are often the source of domain walls, and thicker flakes have a higher probability of containing defects, meaning that thicker flakes are more easily polarized than thinner flakes. As first observed by Kay and Dunn in triglycine sulfate[50], the scaling of E_C with thickness (t) follows the semi-empirical scaling law: $E_C \propto t^{-\frac{2}{3}}$. In the case of our data, if we simply plot (E_C) vs t (using a log-log scale) we observe an empirical relationship $E_C \propto t^{-1}$ (the "uncorrected" data in **Figure 7a**). However, if we apply a depolarization correction to the field data, as discussed by Dawber et al.[47], such that:

$E_C(Corrected) = E_C/(t + 2\delta\varepsilon_{st})$ where t is the thickness of the relevant flake, and δ the thickness of the dead layer (using the model values of δ=0.035nm and ε_{st}=140), then we get the "corrected" plot in **Figure 7a**, which produces an exponent of -0.7, close to the value of 0.66 expected from the Kay and Dunn law.

Finally, we should comment on the observed values of κ and the way these are observed to vary with flake thickness. In a perfect system, we would expect κ=1, so that the polarization induced by the applied field is directly proportional to the field and a constant value of ε_{st} for all flake thicknesses, but this is not the case here. The observed values of κ are plotted as a function of flake thickness in **Figure 7b**. Empirically, we observe that κ is proportional to flake thickness over the full range of flake thicknesses, although there is a fair degree of scatter in the measurements. There are

a range of reasons as to why this might be the case. The effect of field concentration at the PFM tip and the way that interacts with the flake thickness may be one cause of non-linearity and the effects of damage in the oxide at low thicknesses may be another. This is an area for further study.

Discussion and Outlook

We have reported here the fabrication and characterization by various probe microscopies of exfoliated APM B5TFCO nanoflakes. These are either stacked together as multi-flakes or dispersed individually with flake thicknesses ranging from 120nm to 2.4nm. PFM imaging has demonstrated piezoelectricity in both lateral and vertical directions with higher piezoresponses in the lateral (11pmV^{-1}) compared with the vertical (2-3pmV^{-1}), as expected for APMs with the major polarization vector along the *a*-axis. Local PFM switching loops were generated for the nano-sized flakes. The details of the PFM response, including the time-structure in both field-on and field-off states, has been accurately described with a model using charge injection through a Schottky barrier at the electrode-FE oxide interface, in association with charge storage in (and time-dependent leakage from) a surface layer, where the charge injection is affected by the magnitude and sign of the FE polarization. The parameters derived from this model such as permittivities, electrostrictive coefficients, spontaneous polarization magnitudes etc. are all in excellent agreement with values for similar materials taken from the literature. Based on the parameters derived from fitting this model to the data, the coercive field (E_c) scales with thickness (t), following the semi-empirical scaling law: $E_C \propto t^{-\frac{2}{3}}$. It is believed that the balance of evidence obtained from the PFM measurements indicates that room temperature ferroelectricity can exist, and can be switched, in nano-structured B5TFCO flakes as thin as 4.2 and 2.4 nm. The observation of multi-domain structures within single, unpoled nanoflakes which have not undergone PFM-driven switching is supporting evidence for the existence of ferroelectricity in these very thin flakes. The observation of out-of-plane FE switching in such thin flakes for an APM with m=4 is very interesting. Normally, we would not expect to see any component of P_S out of the basal plane of an APM structure for which m is even.[28, 51] Clearly, we see a switchable component of P_S in our measurements. The most-likely explanation is that the

flakes are not lying perfectly parallel to the underlying substrate surface, in which case we would reasonable expect to be able to switch a component of the in-plane polarization. A simple estimate shows that for an in-plane P_S of 0.4Cm^{-2} (as expected for most APM FEs), a flake would only need to be sitting at an angle (Φ) of <6° to give an out-of-plane component of ≈0.04Cm^{-2}, the average value observed in this work. However, the smallest measured values of out-of-plane P_S in Table S1 would correspond to values of Φ≈2.5° and the largest Φ≈10°. Nevertheless, the observed values of the out-of-plane P_S component observed in this work are remarkably consistent from grain to grain, and across the different grain thicknesses, and very similar to the value observed for $Bi_4Ti_3O_{12}$, so the intriguing possibility remains that we are seeing an intrinsic out-of-plane component for P_S, which would mean that the symmetry is not as expected ($A2_1am$),[52] but something lower. This possibility requires further work to resolve. It should be noted that a thickness of 4.2nm corresponds closely to the thickness which would be expected for a single unit cell, while 2.4nm is a thickness corresponding to half the unit cell, plus one Bi_2O_2 layer, or slightly more than half a unit-cell of B5TFCO (see **Figure 1**). The thinnest flake would thus appear to be four perovskite blocks in thickness, sandwiched between two Bi_2O_2 layers. We believe that these are the first PFM measurements on exfoliated APMs. The results are a noteworthy contribution to the fundamental research of both ultra-thin piezoelectric and FE materials and also demonstrate for the first time that wide band-gap oxide FEs can be added to the growing class of 2D materials. This is an important conclusion, as it offers the prospect of incorporating the wide range of useful FE properties, vis: a large switchable, built-in spontaneous polarization, piezoelectricity, pyroelectricity etc. into future electronic devices exploiting 2D materials. In addition, we believe that the model for PFM response presented here will be a useful tool for those working with this technique as a means for characterizing FE behavior in thin materials.

Methods

Highly-oriented polycrystalline ceramics of $Bi_5Fe_{0.5}Co_{0.5}Ti_3O_{15}$ prepared via molten salt synthesis[27] were used as the starting material for the liquid exfoliation process. $Bi_5Ti_3Fe_{0.5}Co_{0.5}O_{15}$ powder was dispersed in an aqueous solution of the surfactant sodium cholate (0.1 $mgml^{-1}$ concentration) using an ultrasonic processor (Sonics VX-750) operating at 75% amplitude for 90 mins. The dispersions were left to settle for 72 hours. The top 50% was then decanted into 2 glass vials and centrifuged (Hettick Mickro 22R) at 500rpm for 30 mins to remove any remaining unexfoliated material. Decantation was carried out by pipetting off the top 50% of each dispersion in a single glass vial. Thin films were made by vacuum filtration immediately after centrifugation. Dispersions were filtered through a nitrocellulose membrane (pore size 25mm) and the deposited films were washed with 400ml of Millipore water to remove surfactant. Films were dried for 20 minutes at 50°C before transfer onto Ti coated SiO_2. Films were wetted with isopropyl alcohol and pressed against the substrate. The cellulose filter was removed by treatment with acetone vapor and subsequent acetone liquid baths. Films were annealed at 800°C to remove any remaining surfactant. Flake morphology was analyzed by scanning electron microscopy (SEM) (Zeiss Ultra Plus SEM and FEI DualBeam Helios NanoLab 600i). Cross-sections of the flakes were prepared for micro-structural analysis using a FEI DualBeam Helios NanoLab 600i SEM/FIB (focused ion beam) (final thinning at 93pA 30kV, final polish 2kV 28pA). Samples were gold-coated to prevent charging. Micro-structural analysis was performed on the B5TFCO flakes using HR-TEM (high resolution transmission electron microscopy; Jeol 2100 transmission electron microscope; 200kV; double tilt holder). Elemental mapping was performed using STEM-EDX (Scanning Transmission Electron Microscopy-Energy Dispersive X-Ray Diffraction; Helios Nanolab STEM - medium spot size, x-ray generation area 10-30 nm in diameter, 100-300 nm lamella thickness). A commercial atomic force microscope (AFM) (MFP-3D™, Asylum Research) was used for topography mapping of the films. Diameter and height values reported in this manuscript were determined by topographical imaging. Electromechanical responses of the films were measured by PFM using an Asylum Research MFP-3D™ AFM in contact mode, equipped with a HVA220 Amplifier for PFM using Single Frequency (drive frequency of 20

kHz) PFM. The angular torsion of the cantilever as it oscillates was monitored in lateral measurements, which were conducted in a similar manner to the vertical measurements except the 'InFast' option was programmed to 'Lateral'. The Dual AC Resonance Tracking Piezoresponse Force Microscopy (DART-PFM)[29] mode was used to boost the vertical piezo signal. In this mode, the PFM signal is measured at the tip-sample contact resonance frequency, where the drive frequencies are adjusted as the probe scans over the changing sample topography in order to reduce topographical cross-talk. Olympus AC240TM Electrilevers, Ti/Pt coated silicon cantilevers (Al reflex coated, 70kHz resonant frequency, ~320kHz contact resonance frequency) were used for PFM and topography imaging. The Inverse Optical Lever Sensitivity of the cantilevers was calibrated according to the MFP-3D Procedural Operation 'Manualette', the system inherent background was determined using a non-piezoelectric silicon wafer and the PFM was then calibrated using α-quartz as a reference sample. Vertical hysteresis loop measurements were obtained at fixed tip positions on the surface of the particles by switching spectroscopy PFM (SS-PFM)[53] using a triangular step waveform (comprised of pulse DC (direct current) bias voltage of 15-35V and an AC (alternating current) drive voltage (V_{ac}) of 5.5V). The waveform was cycled twice at a frequency of 0.3Hz with 55-83 AC steps per waveform. Hysteresis loops taken on a particular flake location were repeated at least three times whereupon repeatable results were obtained.

Author Contributions

R.W.W. proposed the idea of exfoliating APMs into nano-structured flakes and exploring their FE properties. M.P. and A.J.B. synthesized the B5TFCO ceramic sample. R.J.S. and J.N.C. developed the liquid exfoliation method and fabricated the nano-structured B5TFCO flakes. M.S. performed HR-SEM, HR-TEM and STEM-EDX characterization of the B5TFCO flakes. L.K. performed the PFM measurements. R.W.W. devised the model for the PFM response and undertook the modelling of the data. L.K. and R.W.W. wrote the first draft of the manuscript. The final version of the manuscript was written through contributions of all authors. All authors have given approval to the final version of the manuscript.

Notes:

The authors declare no competing financial interest.

Funding Sources

The support of Science Foundation Ireland (SFI) under the FORME Strategic Research Cluster Award number 07/SRC/I1172 is gratefully acknowledged. This publication has emanated from research conducted with the financial support of the Royal Society and Science Foundation Ireland (SFI) University Research Fellowship UF 140263.

References

[1] a) R. Mas-Ballesté, C. Gómez-Navarro, J. Gómez-Herrero, F. Zamora, *Nanoscale* **2011**, 3, 20; b) A. C. Ferrari, F. Bonaccorso, V. Fal'ko, K. S. Novoselov, S. Roche, P. Bøggild, S. Borini, F. H. L. Koppens, V. Palermo, N. Pugno, J. A. Garrido, R. Sordan, A. Bianco, L. Ballerini, M. Prato, E. Lidorikis, J. Kivioja, C. Marinelli, T. Ryhänen, A. Morpurgo, J. N. Coleman, V. Nicolosi, L. Colombo, A. Fert, M. Garcia-Hernandez, A. Bachtold, G. F. Schneider, F. Guinea, C. Dekker, M. Barbone, Z. Sun, C. Galiotis, A. N. Grigorenko, G. Konstantatos, A. Kis, M. Katsnelson, L. Vandersypen, A. Loiseau, V. Morandi, D. Neumaier, E. Treossi, V. Pellegrini, M. Polini, A. Tredicucci, G. M. Williams, B. Hee Hong, J.-H. Ahn, J. Min Kim, H. Zirath, B. J. van Wees, H. van der Zant, L. Occhipinti, A. Di Matteo, I. A. Kinloch, T. Seyller, E. Quesnel, X. Feng, K. Teo, N. Rupesinghe, P. Hakonen, S. R. T. Neil, Q. Tannock, T. Löfwander, J. Kinaret, *Nanoscale* **2015**, 7, 4598.

[2] V. Nicolosi, M. Chhowalla, M. G. Kanatzidis, M. S. Strano, J. N. Coleman, *Science* **2013**, 340.

[3] X. Dong, M. Osada, H. Ueda, Y. Ebina, Y. Kotani, K. Ono, S. Ueda, K. Kobayashi, K. Takada, T. Sasaki, *Chemistry of Materials* **2009**, 21, 4366.

[4] B.-W. Li, M. Osada, T. C. Ozawa, R. Ma, K. Akatsuka, Y. Ebina, H. Funakubo, S. Ueda, K. Kobayashi, T. Sasaki, *Japanese Journal of Applied Physics* **2009**, 48, 09KA15.

[5] M. Osada, T. Sasaki, *Journal of Materials Chemistry* **2009**, 19, 2503.

[6] P. Poizot, S. Laruelle, S. Grugeon, L. Dupont, J. M. Tarascon, *Nature* **2000**, 407, 496.

[7] V. Subramanian, H. Zhu, B. Wei, *Journal of Power Sources* **2006**, 159, 361.

[8] Y. Li, G. Chen, C. Zhou, Z. Li, *Catalysis Letters* **2008**, 123, 80.

[9] Y. Yu, L. Ma, P. Cai, R. Zhong, C. Ye, J. Shen, G. D. Gu, X. H. Chen, Y. Zhang, *Nature* **2019**, 575, 156.

[10] R. W. Whatmore, in *Springer Handbook of Electronic and Photonic Materials*, DOI: 10.1007/978-0-387-29185-7_27, Springer-Verlag, Boston **2007**, p. 597.

[11] J. F. Scott, C. A. Paz de Araujo, *Science* **1989**, 246, 1400.

[12] Q. Su, P. Kirby, E. Komuro, M. Imura, Q. Zhang, R. Whatmore, *IEEE Transactions on Microwave Theory and Techniques* **2001**, 49, 769.

[13] a) R. W. Whatmore, *Reports on Progress in Physics* **1986**, 49, 1335; b) P. Muralt, *Reports on Progress in Physics* **2001**, 64, 1339.

[14] a) S. Palto, L. Blinov, A. Bune, E. Dubovik, V. Fridkin, N. Petukhova, K. Verkhovskaya, S. Yudin, *Ferroelectrics* **1996**, 184, 127; b) L. M. Blinov, V. M. Fridkin, S. P. Palto, A. V. Sorokin, S. G. Yudin, *Thin Solid Films* **1996**, 284-285, 474.

[15] A. Zenkevich, M. Minnekaev, Y. Lebedinskii, K. Bulakh, A. Chouprik, A. Baturin, R. Mantovan, M. Fanciulli, O. Uvarov, *Thin Solid Films* **2012**, 520, 4586.

[16] F. Xue, W. Hu, K.-C. Lee, L.-S. Lu, J. Zhang, H.-L. Tang, A. Han, W.-T. Hsu, S. Tu, W.-H. Chang, C.-H. Lien, J.-H. He, Z. Zhang, L.-J. Li, X. Zhang, *Advanced Functional Materials* **2018**, 28, 1803738.

[17] S. Yuan, X. Luo, H. L. Chan, C. Xiao, Y. Dai, M. Xie, J. Hao, *Nature Communications* **2019**, 10, 1775.

[18] J. J. Gervacio-Arciniega, E. Prokhorov, F. J. Espinoza-Beltrán, G. Trapaga, *Journal of Applied Physics* **2012**, 112, 052018.

[19] B. Aurivillius, *Ark. Kemi.* **1949**, 1, 499.

[20] E. C. Subbarao, *Physical Review* **1961**, 123, 2202.

[21] a) C. A. P. de Araujo, J. D. Cuchiaro, L. D. McMillan, M. C. Scott, J. F. Scott, *Nature* **1995**, 374, 627; b) B. H. Park, B. S. Kang, S. D. Bu, T. W. Noh, J. Lee, W. Jo, *Nature* **1999**, 401, 682.

[22] N. A. Lomanova, I. V. Pleshakov, M. P. Volkov, V. V. Gusarov, *Materials Science and Engineering: B* **2016**, 214, 51.

[23] a) L. Keeney, T. Maity, M. Schmidt, A. Amann, N. Deepak, N. Petkov, S. Roy, M. E. Pemble, R. W. Whatmore, *Journal of the American Ceramic Society* **2013**, 96, 2339; b) A. Faraz, T. Maity, M. Schmidt, N. Deepak, S. Roy, M. E. Pemble, R. W. Whatmore, L. Keeney, *Journal of the American Ceramic Society* **2017**, 100, 975; c) L. Keeney, C. Downing, M. Schmidt, M. E. Pemble, V. Nicolosi, R. W. Whatmore, *Scientific Reports* **2017**, 7, 1737; d) M. Schmidt, A. Amann, L. Keeney, M. E. Pemble, J. D. Holmes, N. Petkov, R. W. Whatmore, *Scientific Reports* **2014**, 4, 5712; e) S. Manipatruni, D. E. Nikonov, C.-C. Lin, T. A. Gosavi, H. Liu, B. Prasad, Y.-L. Huang, E. Bonturim, R. Ramesh, I. A. Young, *Nature* **2019**, 565, 35.

[24] a) V. Chevalller, G. Nihoul, V. Madigou, *Journal of Solid State Chemistry* **2008**, 181, 439; b) S. Ida, C. Ogata, U. Unal, K. Izawa, T. Inoue, O. Altuntasoglu, Y. Matsumoto, *Journal of the American Chemical Society* **2007**, 129, 8956; c) J.-Y. Kim, I. Chung, J.-H. Choy, G.-S. Park, *Chemistry of Materials* **2001**, 13, 2759; d) M. B. Sreedhara, B. E. Prasad, M. Moirangthem, R. Murugavel, C. N. R. Rao, *Journal of Solid State Chemistry* **2015**, 224, 21.

[25] X. Mao, W. Wang, X. Chen, Y. Lu, *Applied Physics Letters* **2009**, 95, 082901.

[26] R. J. Smith, P. J. King, M. Lotya, C. Wirtz, U. Khan, S. De, A. O'Neill, G. S. Duesberg, J. C. Grunlan, G. Moriarty, J. Chen, J. Wang, A. I. Minett, V. Nicolosi, J. N. Coleman, *Advanced Materials* **2011**, 23, 3944.

[27] M. Palizdar, T. P. Comyn, M. B. Ward, A. P. Brown, J. P. Harrington, S. Kulkarni, L. Keeney, S. Roy, M. E. Pemble, R. W. Whatmore, C. Quinn, S. H. Kilcoyne, A. J. Bell, *Journal of Applied Physics* **2012**, 112, 073919.

[28] T. Watanabe, H. Funakubo, *Journal of Applied Physics* **2006**, 100.

[29] B. J. Rodriguez, C. Callahan, S. V. Kalinin, R. Proksch, *Nanotechnology* **2007**, 18, 475504.

[30] B. J. Rodriguez, X. S. Gao, L. F. Liu, W. Lee, I. I. Naumov, A. M. Bratkovsky, D. Hesse, M. Alexe, *Nano Letters* **2009**, 9, 1127.

[31] B. J. Rodriguez, S. Jesse, M. Alexe, S. V. Kalinin, *Advanced Materials* **2008**, 20, 109.

[32] L. Keeney, S. Kulkarni, N. Deepak, M. Schmidt, N. Petkov, P. F. Zhang, S. Cavill, S. Roy, M. E. Pemble, R. W. Whatmore, *Journal of Applied Physics* **2012**, 112, 052010.

[33] R. K. Vasudevan, N. Balke, P. Maksymovych, S. Jesse, S. V. Kalinin, *Applied Physics Reviews* **2017**, 4, 021302.

[34] S. Jesse, H. N. Lee, S. V. Kalinin, *Review of Scientific Instruments* **2006**, 77, 073702.

[35] E. Strelcov, Y. Kim, J. C. Yang, Y. H. Chu, P. Yu, X. Lu, S. Jesse, S. V. Kalinin, *Applied Physics Letters* **2012**, 101, 192902.

[36] a) H. Bo, Y. Kan, X. Lu, S. Peng, X. Wang, Y. Liu, W. Cai, R. Xue, J. Zhu, *Review of Scientific Instruments* **2010**, 81, 043704; b) S. V. Kalinin, B. J. Rodriguez, S. Jesse, J. Shin, A. P. Baddorf, P. Gupta, H. Jain, D. B. Williams, A. Gruverman, *Microscopy and Microanalysis* **2006**, 12, 206.

[37] B. Kim, F. P. Barrows, Y. Sharma, R. S. Katiyar, C. Phatak, A. K. Petford-Long, S. Jeon, S. Hong, *Scientific Reports* **2018**, 8, 203.

[38] H. W. Jang, A. Kumar, S. Denev, M. D. Biegalski, P. Maksymovych, C. W. Bark, C. T. Nelson, C. M. Folkman, S. H. Baek, N. Balke, C. M. Brooks, D. A. Tenne, D. G. Schlom, L. Q. Chen, X. Q. Pan, S. V. Kalinin, V. Gopalan, C. B. Eom, *Physical Review Letters* **2010**, 104, 197601.

[39] R. P. Ummer, R. B, C. Thevenot, D. Rouxel, S. Thomas, N. Kalarikkal, *RSC Advances* **2016**, 6, 28069.

[40] L. Pintilie, M. Alexe, *Journal of Applied Physics* **2005**, 98, 124103.

[41] Z. Fan, H. Fan, Z. Lu, P. Li, Z. Huang, G. Tian, L. Yang, J. Yao, C. Chen, D. Chen, Z. Yan, X. Lu, X. Gao, J.-M. Liu, *Physical Review Applied* **2017**, 7, 014020.

[42] S. L. Miller, R. D. Nasby, J. R. Schwank, M. S. Rodgers, P. V. Dressendorfer, *Journal of Applied Physics* **1990**, 68, 6463.

[43] P. W. M. Blom, R. M. Wolf, J. F. M. Cillessen, M. P. C. M. Krijn, *Physical Review Letters* **1994**, 73, 2107.

[44] K. W. Kwok, H. Y. Wong, *Journal of Physics D: Applied Physics* **2009**, 42, 095419.

[45] T. Takenaka, K. Sakata, *Journal of Applied Physics* **1984**, 55, 1092.

[46] S. E. Cummins, L. E. Cross, *Journal of Applied Physics* **1968**, 39, 2268.
[47] M. Dawber, P. Chandra, P. B. Littlewood, J. F. Scott, *Journal of Physics: Condensed Matter* **2003**, 15, L393.
[48] K. Uchino, L. E. Cross, R. E. Newnham, S. Nomura, *Phase Transitions* **1980**, 1, 333.
[49] S. Ducharme, V. M. Fridkin, A. V. Bune, S. P. Palto, L. M. Blinov, N. N. Petukhova, S. G. Yudin, *Physical Review Letters* **2000**, 84, 175.
[50] H. F. Kay, J. W. Dunn, *The Philosophical Magazine: A Journal of Theoretical Experimental and Applied Physics* **1962**, 7, 2027.
[51] a) R. E. Newnham, R. W. Wolfe, J. F. Dorrian, *Materials Research Bulletin* **1971**, 6, 1029; b) H. Irie, M. Miyayama, *Applied Physics Letters* **2001**, 79, 251.
[52] C. H. Hervoches, A. Snedden, R. Riggs, S. H. Kilcoyne, P. Manuel, P. Lightfoot, *Journal of Solid State Chemistry* **2002**, 164, 280.
[53] a) S. Jesse, A. P. Baddorf, S. V. Kalinin, *Appl. Phys. Lett.* **2006**, 88, 062908; b) S. Jesse, H. N. Lee, S. V. Kalinin, Vol. 77, AIP, 2006, 073702.

Figures

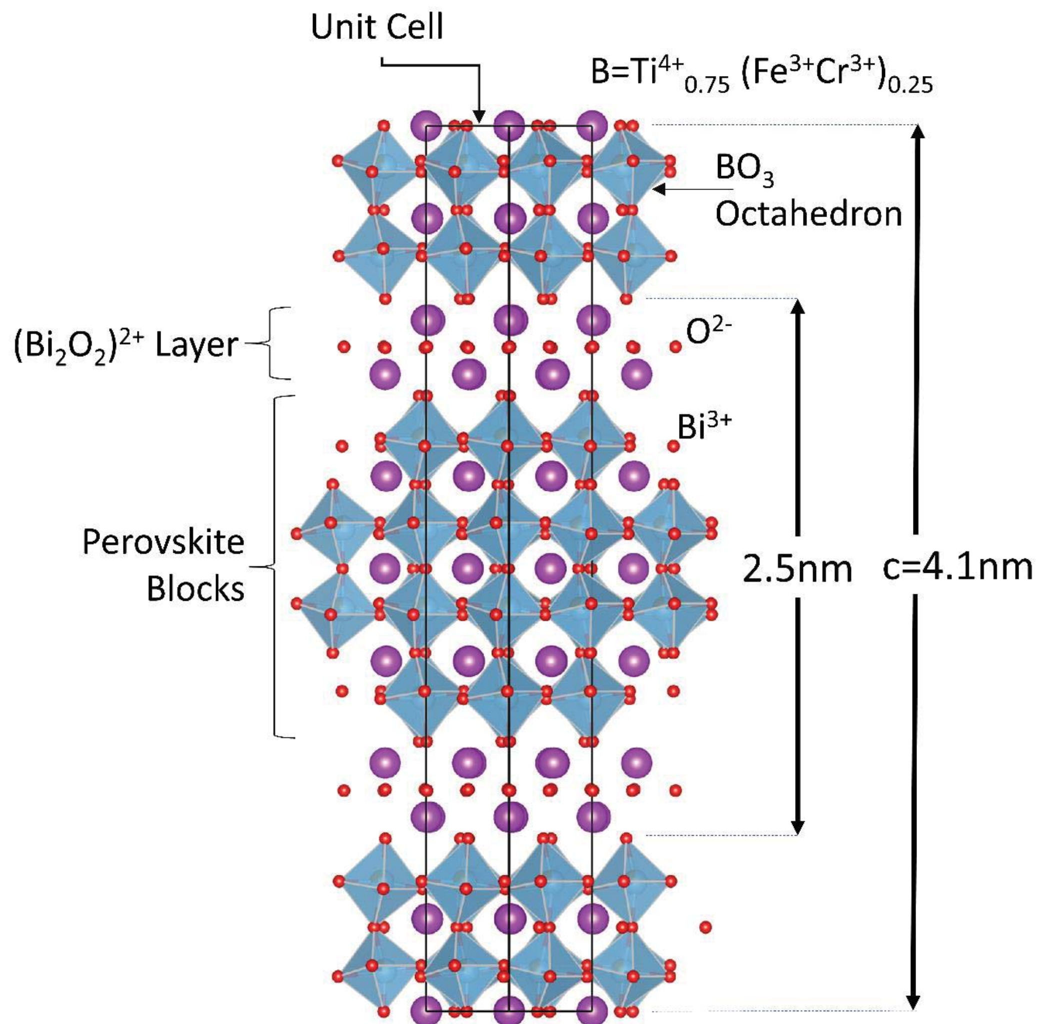

Figure 1: Schematic diagram of the B5TFCO APM structure, viewed approximately along [110], illustrating the main structural features and the relevant unit cell dimensions.

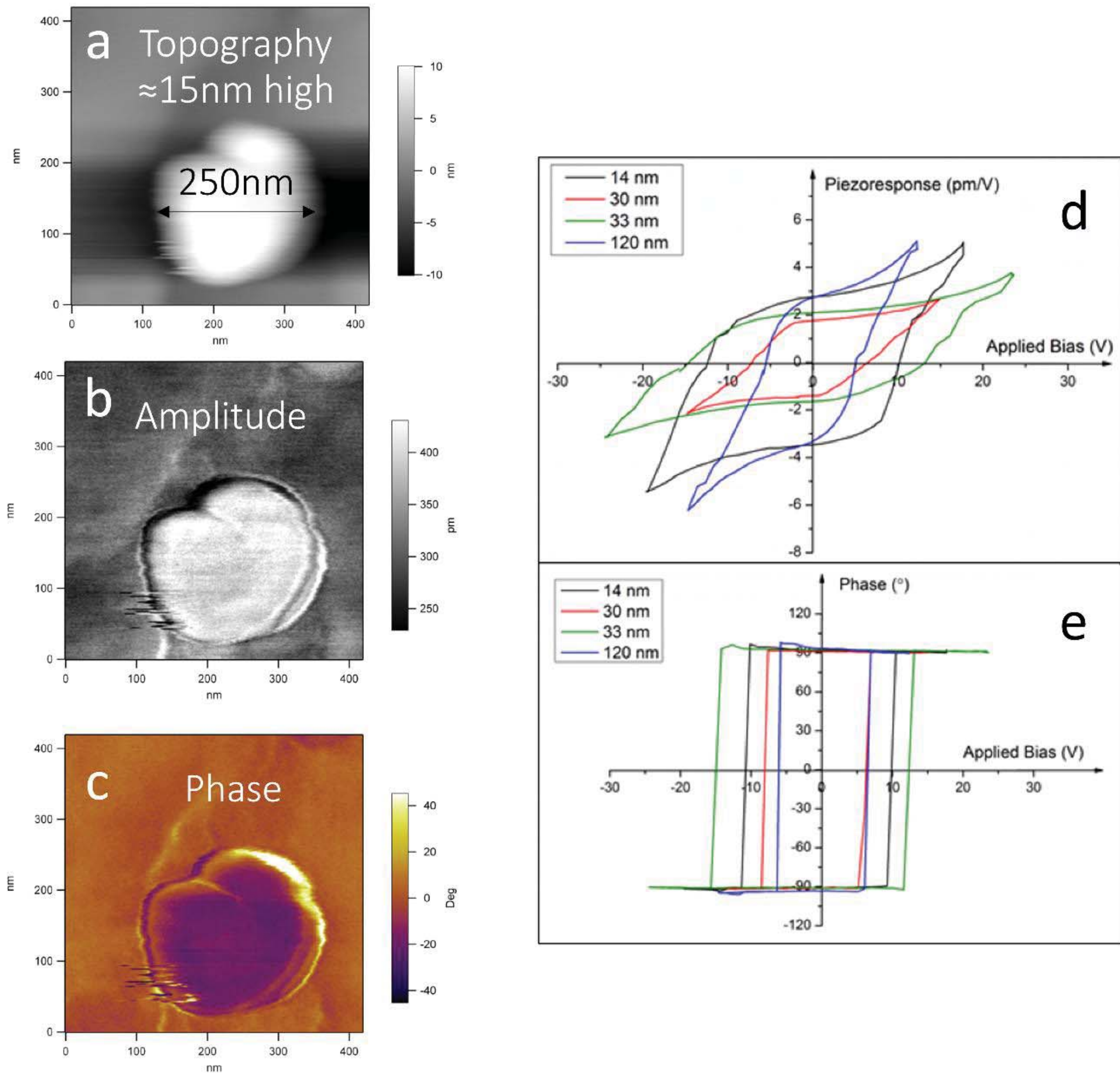

Figure 2. Representative **a.** topography, **b.** vertical DART-PFM amplitude and **c.** vertical DART-PFM phase images of a single 15nm-high flake of exfoliated B5TFCO. Vertical DART-PFM switching spectroscopy **h** piezoresponse and **i** phase loops of exfoliated B5TFCO nanoflakes at room temperature after removal of an applied DC bias.

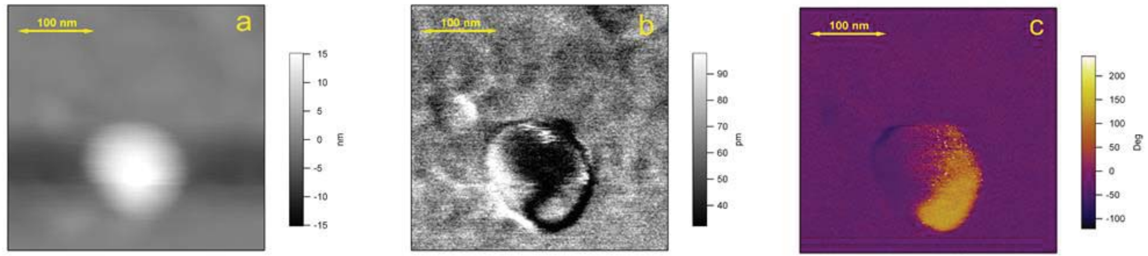

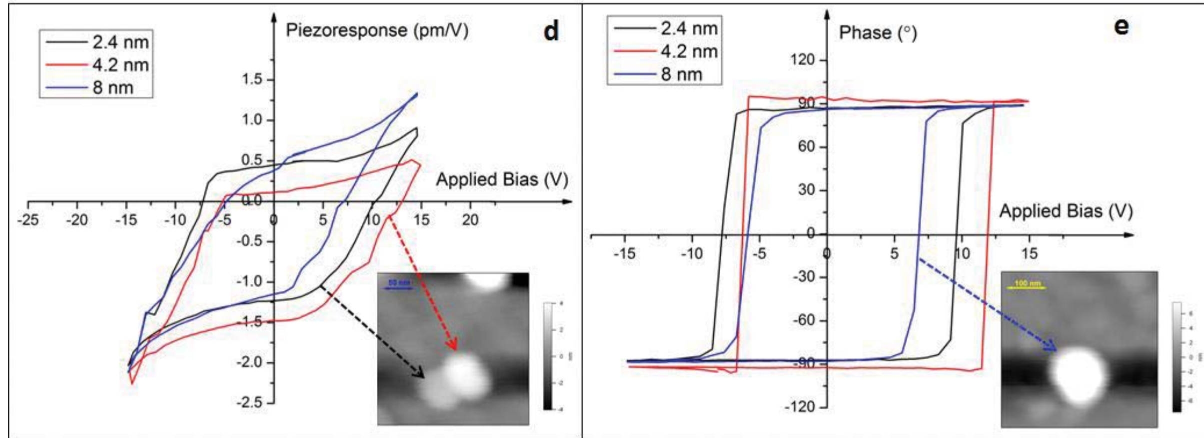

Figure 3. Representative **a** topography, **b** vertical DART-PFM amplitude and **c** vertical DART-PFM phase images of an individual exfoliated 8nm thick B5TFCO flake. Vertical DART-PFM switching spectroscopy **d** piezoresponse and **e** phase loops of individual exfoliated B5TFCO flakes at room temperature after removal of an applied DC bias. The topography of flakes with height 2.4 nm and 4.2 nm are shown in the inset in **d** and the topography of flake with height 8nm is shown in the inset in **e**.

1
2
3
4
5
6
7
8
9
10
11
12
13
14
15
16
17
18
19
20
21
22
23
24
25
26
27
28
29
30
31
32
33
34
35
36
37
38
39
40
41
42
43
44
45
46
47
48
49
50
51
52
53
54
55
56
57
58
59
60
61
62
63
64
65

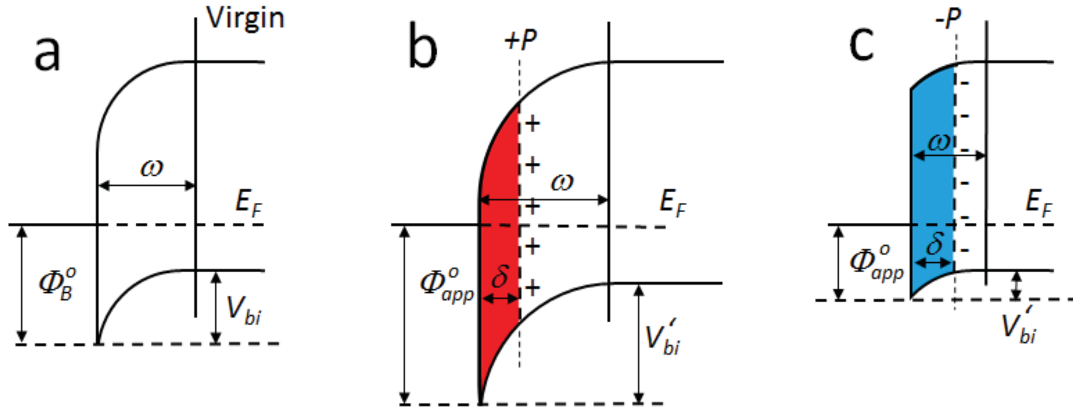

Figure 4. Energy band diagrams of a Schottky diode in **a** virgin (without polarization and trapped charges), **b** negatively poled and **c** positively poled states (redrawn with permission from Fan et al. 2017, American Physical Society[41]).

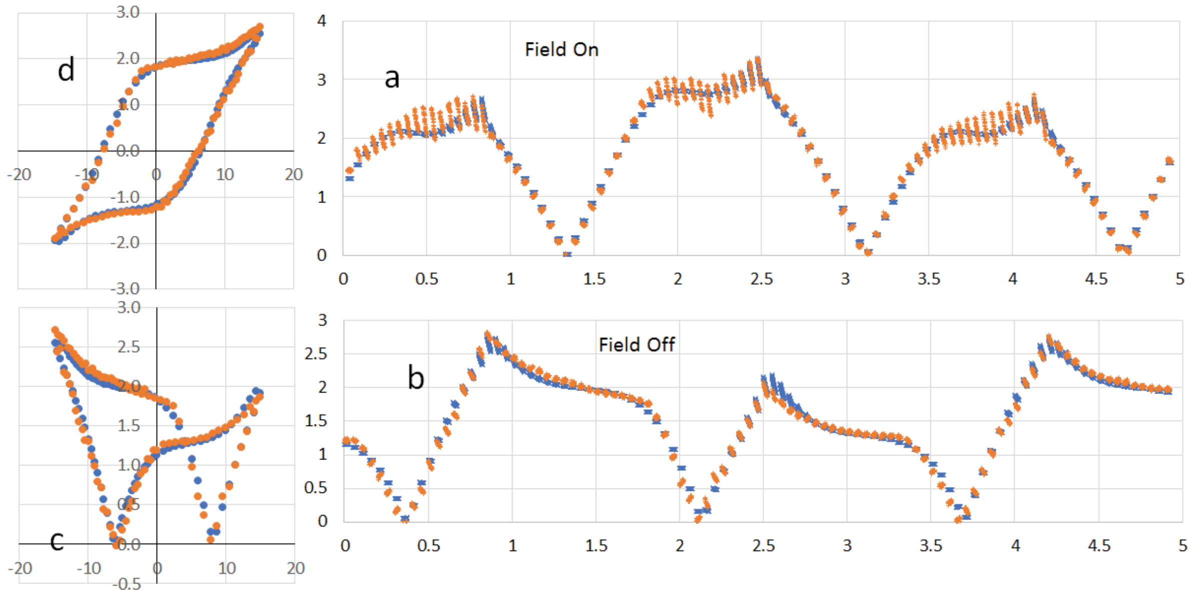

Figure 5. Results of fitting the parameters as discussed in the text for a 30nm thick B5TFCO flake. This shows **a** Field-on and **b** Field-off time responses in pmV^{-1}. In each case the horizontal axes are plotted in seconds. **c** Butterfly and **d** Hysteresis loops in pmV^{-1} plotted vs applied voltage. In each case, the observed data is plotted in orange and the modelled data in blue.

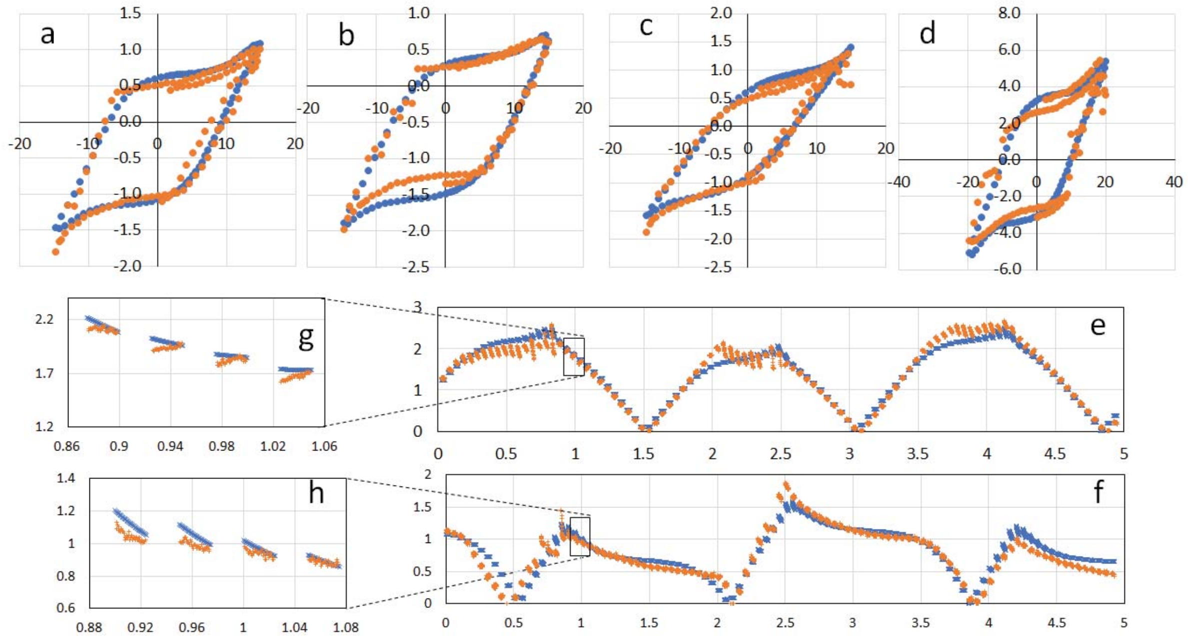

Figure 6. Comparison of measured and modelled PFM piezoresponse hysteresis loops for **a** 2.4nm, **b** 4.2nm, **c** 8nm and **d** 14nm exfoliated B5TFCO flakes. In each case the piezoresponse (vertical axes) is measured in pmV^{-1} and the applied voltage (horizontal axes) in volts. Figures **3 e** and **f** show respectively the field-on and field-off time structures of the piezoresponse signals (in pmV^{-1}) for the 2.4nm flake. Figures **3 g** and **h** show respectively magnified sections of the field-on and field-off time structures of the piezoresponse signals (in pmV^{-1}) for the 2.4nm flake. The horizontal axes are plotted in seconds. In each case, the observed data is plotted in orange and the model data is plotted in blue.

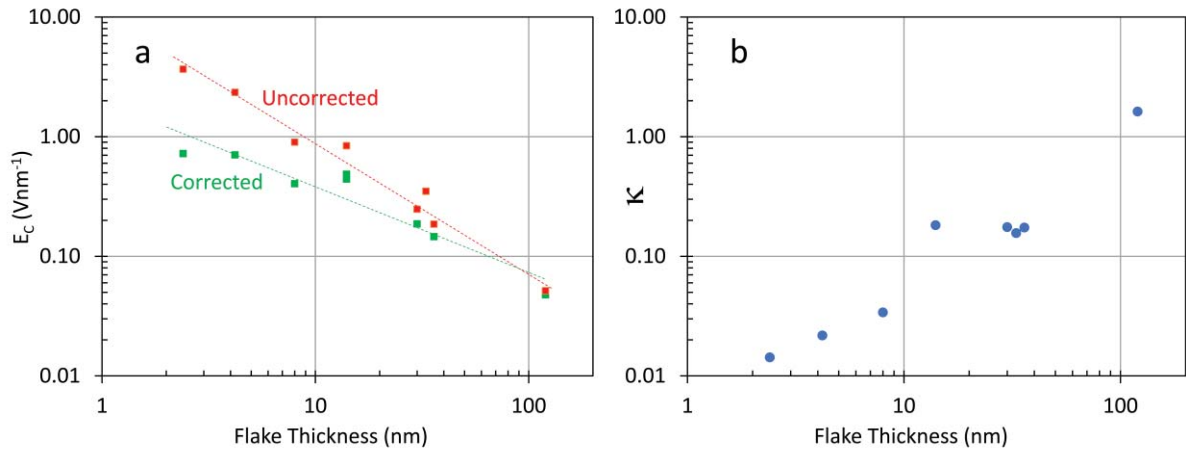

Figure 7. a Log-log plots of the uncorrected and corrected coercive fields vs flake thickness and **b** Log-log plot of the variable k vs flake thickness as derived from the fits of the model to the measured piezoresponse data.

Flake Thickness nm	V_{Max} Volts	V_C Volts	E_C MVm^{-1}	V_{shift} Volts	P_S Cm^{-2}	ΔP_R Cm^{-2}	P_{shift} Cm^{-2}	Decay Const s^{-1}	Drift Mobility $m^2V^{-1}s^{-1}$	κ	ElectroStr Coeff't m^4C^{-2}	r^2
2.4	15.0	8.80	3,667	0.09	0.032	0.0021	-0.007	13.90	9.60E-07	0.014	0.021	0.01250
4.2	15.0	9.85	2,345	-0.48	0.031	0.0029	-0.015	19.00	9.00E-07	0.022	0.021	0.00961
8.0	15.0	7.19	899	0.22	0.030	0.0090	-0.003	54.00	3.10E-06	0.034	0.022	0.01566
14.0	15.0	10.50	839	0.05	0.085	0.0085	0.003	14.00	7.90E-07	0.182	0.020	0.03105
30.0	15.0	7.42	247	-0.06	0.036	0.0032	0.007	15.00	1.19E-06	0.175	0.020	0.00309
33.0	15.0	7.50	227	0.19	0.018	0.0005	-0.002	12.30	1.00E-06	0.134	0.021	0.01396
33.0	17.5	10.15	308	0.00	0.022	0.0001	-0.01	11.60	5.00E-07	0.155	0.020	0.00763
33.0	20.0	12.41	376	0.24	0.026	0.0000	0.00	12.30	3.00E-07	0.167	0.020	0.00825
33.0	22.5	11.45	347	0.26	0.026	0.0002	0.00	8.94	1.15E-07	0.142	0.020	0.02322
33.0	25.0	13.68	415	-0.27	0.034	0.0011	-0.01	7.00	7.30E-08	0.151	0.019	0.01689
33.0	25.0	14.05	426	0.45	0.050	0.0037	0.01	15.40	1.69E-07	0.188	0.020	0.01260
36.0	15.0	6.68	186	0.06	0.027	0.0058	-0.01	23.10	1.85E-06	0.174	0.021	0.00935
120.0	15.0	6.17	51	0.28	0.078	0.0158	0.00	28.15	7.50E-06	1.621	0.021	0.01340

Table S1: Parameters derived from the modelling of the time dependence of the piezoelectric coefficients measured via PFM.

1
2
3
4
5
6
7
8
9
10
11
12
13
14
15
16
17
18
19
20
21
22
23
24
25
26
27
28
29
30
31
32
33
34
35
36
37
38
39
40
41
42
43
44
45
46
47
48
49
50
51
52
53
54
55
56
57
58
59
60
61
62
63
64
65

Ferroelectric Behavior in Exfoliated 2D Aurivillius Oxide Flakes of Sub-Unit Cell Thickness

Supporting Information

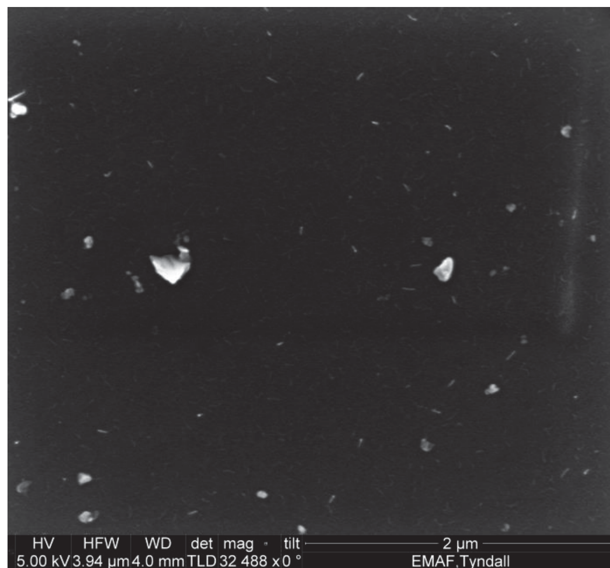

Figure S1. Supporting Information: Representative top-view HRSEM image of exfoliated B5TFCO flakes.

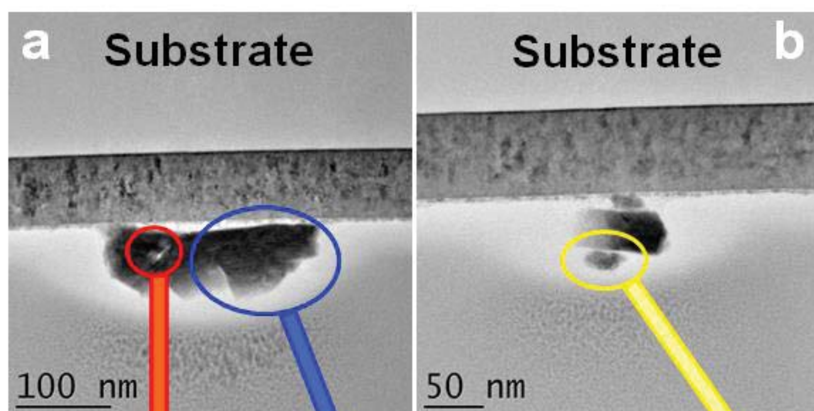

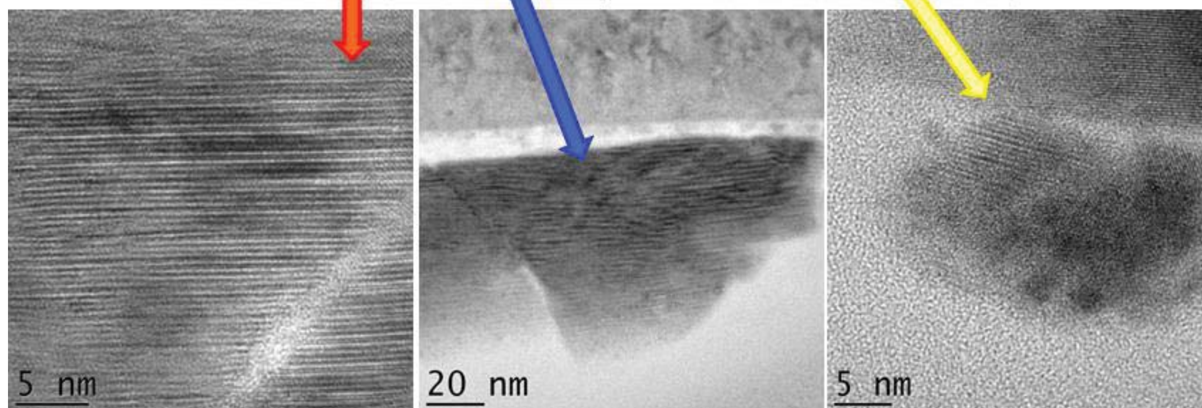

Figure S2. Cross-sectional TEM images of exfoliated B5TFCO flakes. HRTEM of a larger horizontal cluster of multi-flakes (maximum thickness of 80nm and diameter of 230nm) **a** and HRTEM of a smaller vertical multi-flake stack (maximum thickness of 65nm and diameter of 80nm) **b**.

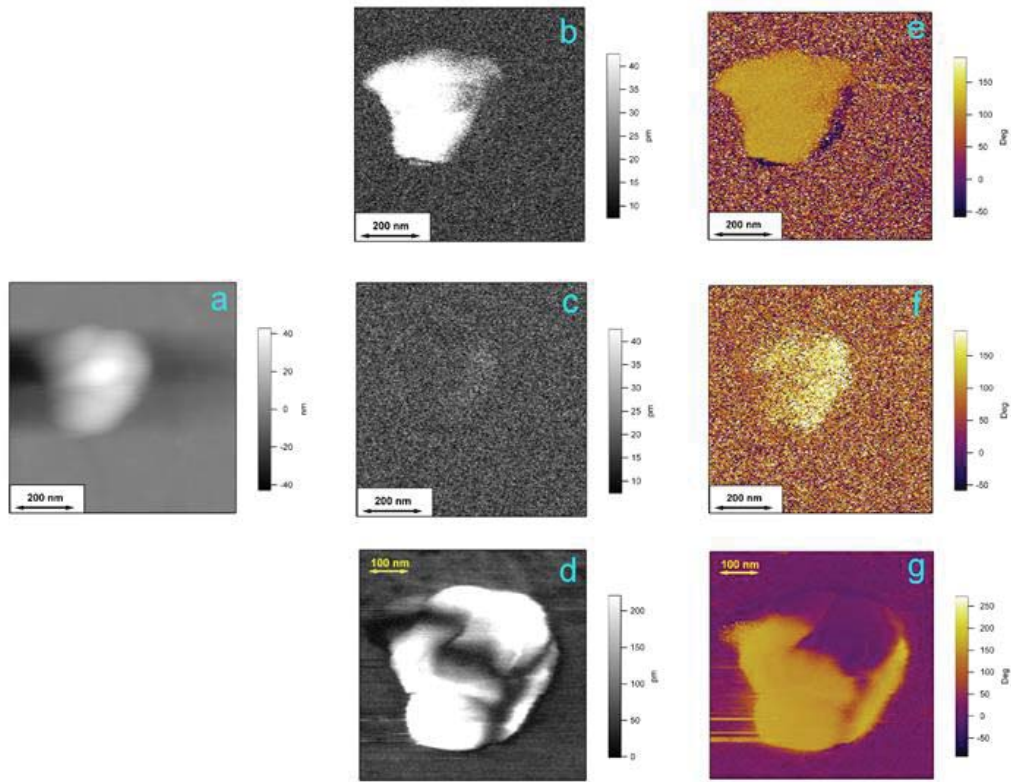

Figure S3. Representative **a.** topography, **b.** lateral single frequency PFM amplitude, **e.** lateral single frequency PFM phase, **c.** vertical single frequency PFM amplitude and **f.** vertical single frequency PFM phase **d.** vertical DART-PFM amplitude and **g.** vertical DART-PFM phase images of a multi-flake cluster of exfoliated B5TFCO.

1
2
3
4
5
6
7
8
9
10
11
12
13
14
15
16
17
18
19
20
21
22
23
24
25
26
27
28
29

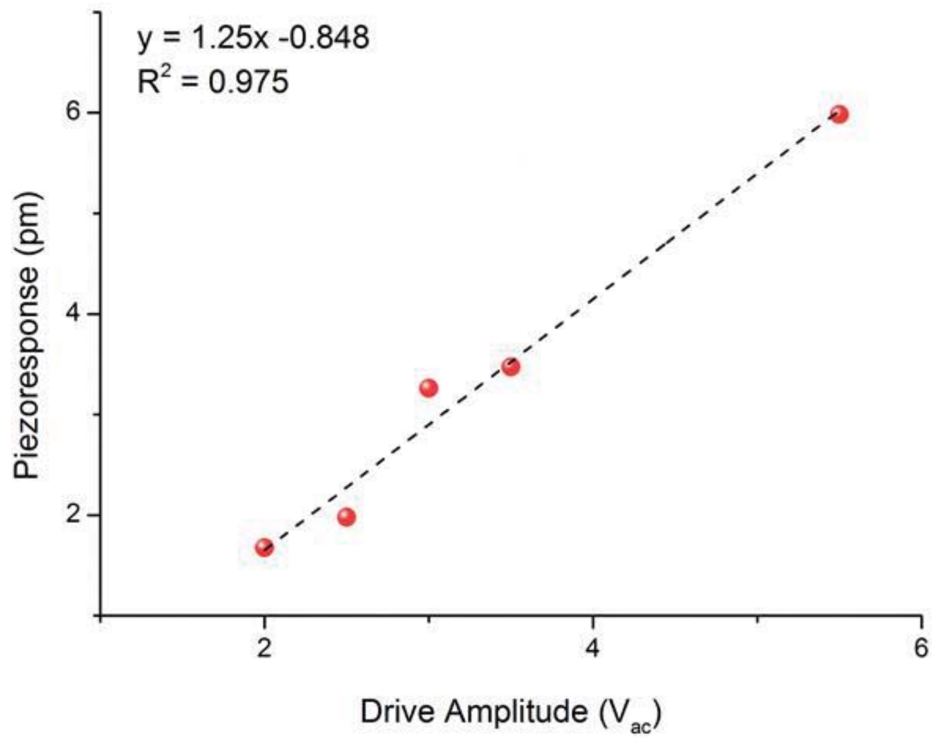

30 **Figure S4.** Piezoresponse as measured by vertical DART-PFM switching spectroscopy as a function of
31
32 drive voltage (2.0 to 5.5V) at a constant DC bias of 15V. Note that the piezoresponse has not been
33
34
35 normalized to pmV^{-1}, it has been displayed in picometers (pm) to allow for the change in
36
37 piezoresponse as a function of voltage to be demonstrated.
38
39
40
41
42
43
44
45
46
47
48
49
50
51
52
53
54
55
56
57
58
59
60
61
62
63
64
65

PFM Response Modelling

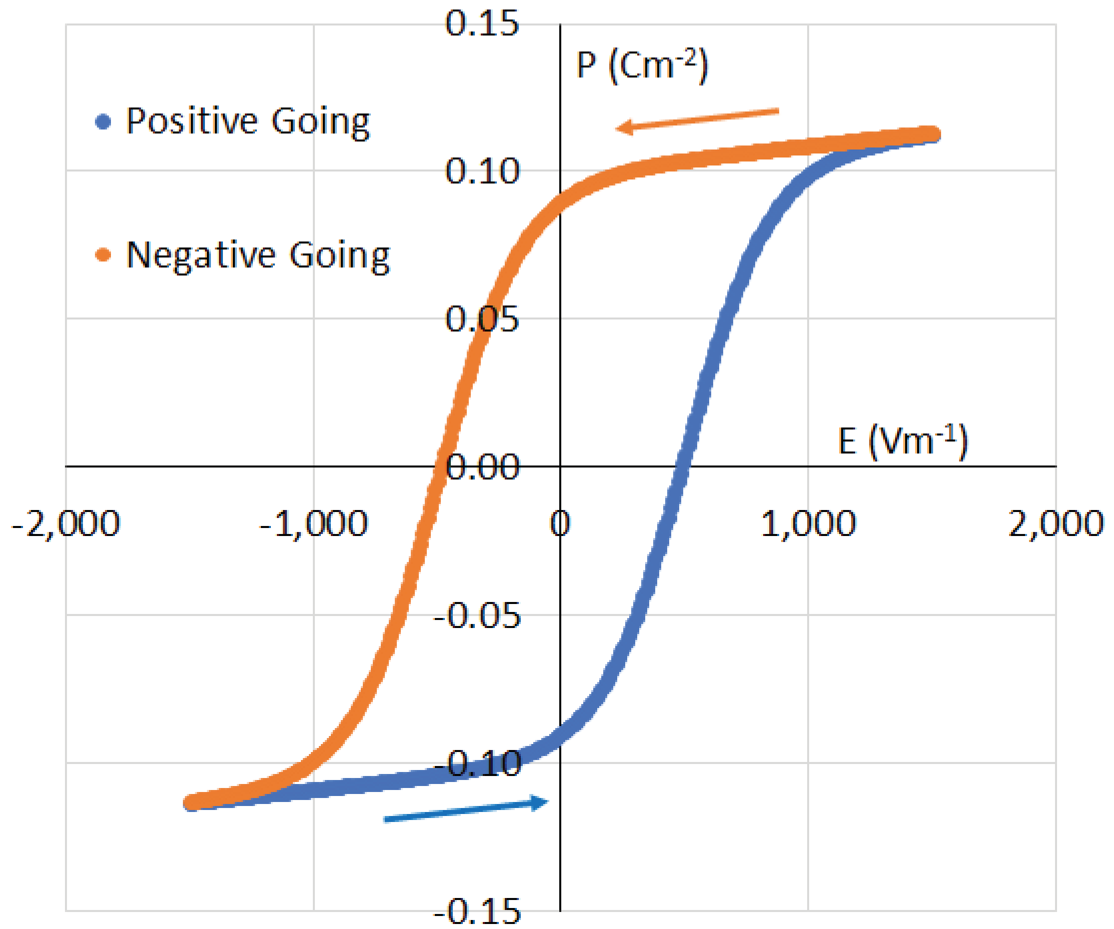

Figure S5. Model of ferroelectric hysteresis based on the function shown in Equation (S18) and (S19).

(P_S=0.1Cm^{-2}, P_R=0.09Cm^{-2}, E_c=500Vm^{-1}, ε_{opt} =2).